Sensors & Actuators: B. Chemical 417 (2024) 136163

Contents lists available at ScienceDirect

Sensors and Actuators: B. Chemical

journal homepage: www.elsevier.com/locate/snb

Surface plasmon resonance biosensor with anti-crossing modulation readout

Roger Hasler [a], Dario Cattozzo Mor [b,c], Gizem Aktug [b,c], Stefan Fossati [b], Van Truc Vu [d], Adrián Tamayo [e], Elena Giordani [f], Elena Ricciardi [f], Patrizio Giacomini [g], Jiri Perutka [h], Kamil Onder [h], Christoph Kleber [a], Paolo Samorì [e], Chun-Jen Huang [d,i], Jakub Dostalek [a,b,*]

[a] Laboratory for Life Sciences and Technology (LiST), Faculty of Medicine and Dentistry, Danube Private University, Krems 3500, Austria
[b] FZU-Institute of Physics, Czech Academy of Sciences, Prague 182 21, Czech Republic
[c] Department of Biophysics, Chemical and Macromolecular Physics, Faculty of Mathematics and Physics, Charles University, Prague 121 16, Czech Republic
[d] Department of Chemical & Materials Engineering, National Central University, Jhong-Li, Taoyuan 320, Taiwan
[e] Université de Strasbourg, CNRS, Institut de Science et d'Ingénierie Supramoléculaires, 8 allée Gaspard Monge, Strasbourg 67000, France
[f] UOC Translational Oncology, IRCCS Regina Elena National Cancer Institute, Rome 00144, Italy
[g] UOSD Medicina di Precisione in Senologia, Fondazione Policlinico Universitario Agostino Gemelli IRCCS, Rome 00168, Italy
[h] Procomcure Biotech, Breitwies 1, Thalgaum 5303, Austria
[i] R&D Center for Membrane Technology, Chung Yuan Christian University, 200 Chung Pei Rd., Chung-Li City 32023, Taiwan

ARTICLE INFO

Keywords:
Surface plasmon resonance
Grating-coupled surface plasmon resonance
Multi-periodic grating
Nanoimprint lithography
Biosensor
Multiplexing
Antifouling biointerface

ABSTRACT

A novel approach to surface plasmon resonance (SPR) biosensors providing simplified label-free monitoring of biomolecular affinity binding events is reported. It is based on the interrogation of anti-crossing surface plasmon modes traveling along opposite interfaces of a thin metal film on the top of a tailored multi-periodic grating structure. It allows for diffraction-based backside excitation of surface plasmons without the need of optical matching of the sensor chip to a prism and it allows avoiding of optical probing through the analyzed liquid sample. In conjunction with low angular dispersion of resonantly excited surface plasmon modes, it provides sensitive and versatile optical interrogation of SPR changes associated with biomolecular binding-induced refractive index variations. Direct readout with a fiber optic probe, as well as multi-channel configuration compatible with regular SPR readers, is implemented with the use of sensor chips prepared by mass production-compatible UV-nanoimprint lithography. The potential of the reported SPR sensor chips is illustrated by its ability to characterize affinity interaction of antibodies specific to cancer biomarker CSPG4 on antifouling mixed thiolated self-assembled monolayer with zwitterionic carboxybetaine and sulfobetaine headgroups.

1. Introduction

SPR biosensors represent an established technology that routinely serves in biomolecular interaction analysis and for the investigation of biointerfaces. It allows measuring the kinetics of biomolecular interactions when one of the molecules, i.e. receptor, is attached to a solid (mostly Au) sensor surface and the affinity partner, i.e. analyte, is present in an aqueous liquid sample that is contacted with this surface. Association and dissociation of biomolecular complexes at the sensor surface leads to variations of surface mass density and it is followed in real-time by monitoring the respective changes in refractive index without the need of labeling of biomolecules. In further development of this method, among others, two important directions have been pursued. The first relies on the implementation of SPR readout optics to portable devices that can be employed for the direct analysis of target analytes outside specialized laboratories, particularly in the context of point-of-care diagnosis [1], environmental monitoring [2] or food safety [3]. These efforts concern novel instrumentation of miniaturized and simplified setups [4–8] in close connection to research on advanced biofunctional antifouling coatings that are essential for mitigation of nonspecific sorption of abundant molecules masking the specific sensor response [9,10]. The second consists in extending the SPR-based probing of surface mass density changes (that are proportional to refractive index variations) to multimodal sensing systems that combine different

* Corresponding author at: FZU-Institute of Physics, Czech Academy of Sciences, Prague 182 21, Czech Republic.
E-mail address: dostalek@fzu.cz (J. Dostalek).

https://doi.org/10.1016/j.snb.2024.136163
Received 12 April 2024; Received in revised form 6 June 2024; Accepted 18 June 2024
Available online 18 June 2024

bioanalytical transducer principles [11,12]. Such multimodal sensing is motivated by the possibility of studying distinct physicochemical characteristics of biointerfaces and affinity interactions in parallel as well as by the need of improving the sensitivity of the involved sensing principles. Among others, multimodal SPR biosensors were reported in combination with field-effect transistor [13,14], electrochemical readout [15], quartz crystal microbalance [16], and vibrational optical spectroscopy such as surface-enhanced Raman spectroscopy [17].

Most commonly, SPR biosensors are constructed with the use of attenuated total reflection (ATR) method in Kretschmann configuration that allows for the phase-matching of an incident optical beam with propagating surface plasmon (PSP) waves. In ATR–based SPR biosensors, there is typically used a permanent prism with optically matched disposable sensor chip carrying a thin metallic layer [18] or more complex multilayer structures for multichannel and self-referenced configurations [19,20]. An alternative approach to ATR-based SPR biosensor measurements that does not require the optical matching has been reported based on disposable fiber optic probes [21]. In addition, SPR with grating coupling element offers also a means to avoid using of optical prisms through diffraction-based excitation of PSPs on periodically corrugated metallic surfaces. These corrugations can be prepared with mass production-compatible techniques and offer a straightforward route for multiplexing of arrays of sensing spots on a sensor chip surface [22] with a possibility to engineer supported surface plasmon modes to implement self-referenced measurements [23,24]. However, grating-coupled SPR with conformally corrugated continuous metallic films imposes a disadvantage associated with the necessity of optical probing through the analyzed liquid sample contacted with the sensor surface, which complicates the design of the microfluidic device used for the sample transportation. The possible backside excitation of surface plasmon waves (through the substrate sensor chip from the opposite side to the sensor surface) was reported for metallic nanoparticles supporting localized surface plasmons (LSPs) [25] or, as recently reported, for PSPs on a continuous Au film corrugated with a multi-diffractive grating [26].

SPR changes are evaluated in majority of SPR biosensor implementations from angular or wavelength reflectivity spectra [27,28]. SPR manifests itself as a narrow dip centered at the resonant SPR wavelength or the SPR angle of incidence and their shifts induced by the changes in refractive index are monitored in time. In order to resolve small changes in refractive index associated with minute SPR shifts, approaches based on centroid tracking [29,30] and polynomial fitting [29] were applied. It is worth of noting that also other methods utilizing SPR dip width tracking [31], a combination of evaluating spectral shift and shape of SPR dip [32], and conversion to color hue change [33] have been explored for a more sensitive or simplified readout of SPR changes.

In this paper, we report on sensitive tracking of molecular binding-induced changes in refractive index that relies on a tailored multi-period diffractive grating (MPG) facilitating anti-crossing modulation of surface plasmon resonance (ACM-SPR). It serves for backside PSP excitation and allows for spectral interrogation of SPR changes with a non-collimated polychromatic optical beam, which enables versatile implementation to various optical configurations. The performance of the sensor is demonstrated in a multichannel system adapted from regular ATR-SPR biosensor as well as in single-channel fiber optic systems, when applied for the readout of layer-by-layer (LbL) deposition and biomolecular affinity interaction analysis. The processing of acquired spectra featuring two SPR dips with opposite sensitivity to refractive index changes is carried out and demonstrated to offer a resolution comparable to other established SPR biosensor systems. In addition, it is employed to aid the development of an immunoassay-based detection of cancer biomarker on top of a self-assembled anti-fouling biointerface bearing functional zwitterionic groups.

2. Methods

2.1. Chemicals

Phosphate buffer saline tablets (PBS: 137 mM NaCl, 10 mM phosphate, 2.7 mM KCl, pH = 7.4), bovine serum albumin (BSA), Tween-20, potassium chloride (≥99 %), poly(diallyldimethylammonium chloride) (PDADMAC, low molecular weight, average weight < 100.000 Da), poly (sodium 4-styrenesulfonate) (PSS, low molecular weight, average weight ≈ 70.000 Da), and Hellmanex™ III solution were obtained from Sigma (Germany). PBS-Tween-BSA was prepared by adding Tween20 (0.05 %) and BSA (0.1 %) to PBS solution. N-(3-Dimethylaminopropyl)-N′-ethylcarbodiimide hydrochloride (EDC hydrochloride) and N-Hydroxysuccinimide (NHS) were purchased from Merck (Germany). Ethanol (96 %) and ethanol absolute (≥99.8 %) were obtained from Penta (Czechia). Ethanolamine (1 M, pH 8.5) was acquired from Cytiva (USA). All buffer solutions were prepared by using ultrapure water (Direct-Q 3UV, Merck, Germany).

2.2. Biomaterials

Human CSPG4 protein was expressed in suspension CHO stable cell culture. The cell culture broth was centrifuged, and the protein-rich supernatant was purified by affinity chromatography using a HisTrap™ FF Crude column. After washing and elution with appropriate buffers, the eluted fractions were pooled, and the buffer was exchanged to PBS, pH 7.2. Next, the target protein was loaded onto the HiLoad™ 26/600 Superdex 200 pg 320 mL column, and fractions with higher purity were combined. The purified CSPG4 protein was subsequently analyzed by SDS-PAGE and SEC-HPLC, determining an estimated molecular weight of ~250 kDa. Murine antibodies against chondroitin sulfate proteoglycan 4-(CSPG4), Ep2 and Ep3, were prepared according to a previously reported procedure [34].

2.3. Preparation of sensor chips

ACM-SPR sensor chips with MPG were prepared from a master structure developed in our previous work [26] as schematically shown in Fig. 1. The MPG corrugation profile on the master structure was casted to a soft polydimethylsiloxane (PDMS, from DOW Europe GmbH) stamp by using curing at room temperature (RT = 20–22°C) (3 days) or elevated temperature of 60°C (overnight). The cured PDMS stamp was detached from the master substrate, leaving a negative copy of the MPG structure in the PDMS. BK7 glass substrates (1 mm in thickness) were cut to a dimension of 2×2 cm^2 and cleaned by subsequent sonication for 15 min in a 1 % Hellmanex TM III aqueous solution, 15 min in ultrapure water, and 15 min in ethanol. Amonil MMS10 (from AMO GmbH, Germany) was spun on cleaned glass substrates at 3000 rpm for 120 s. The PDMS working stamp was placed on top of the Amonil layer to imprint the MPG structure. After a resting time of 5 min, the Amonil layer was irradiated by UV light at 365 nm with a dose of 2 J cm^{-2} (UV lamp Bio-Link 365, Vilber Lourmat). The PDMS working stamp was then detached from the UV-cured Amonil layer, leaving a copy of the MPG master structure. The substrates with Amonil MPG were then coated with a thin adhesion promoting Cr (thickness of d_{Cr} = 0.5–2 nm) and Au (thickness of d_{Au} = 50 nm) layers by thermal evaporation (Plassys MEB 300) with a pre-vacuum of 2•10^{-7} mbar and a coating rate of 0.03 nm s^{-1}.

2.4. Morphological characterization

Topography of prepared sensor chips was measured with atomic force microscopy (AFM) by using a Bruker Dimension Icon set-up, operating in tapping mode and using TESPA-V2 tips with tip stiffness of 42 N m^{-1} in air. The 5×5 μm^2 images were captured at a scan rate of 0.98 Hz with a resolution of 1024×1024 pixels per image.

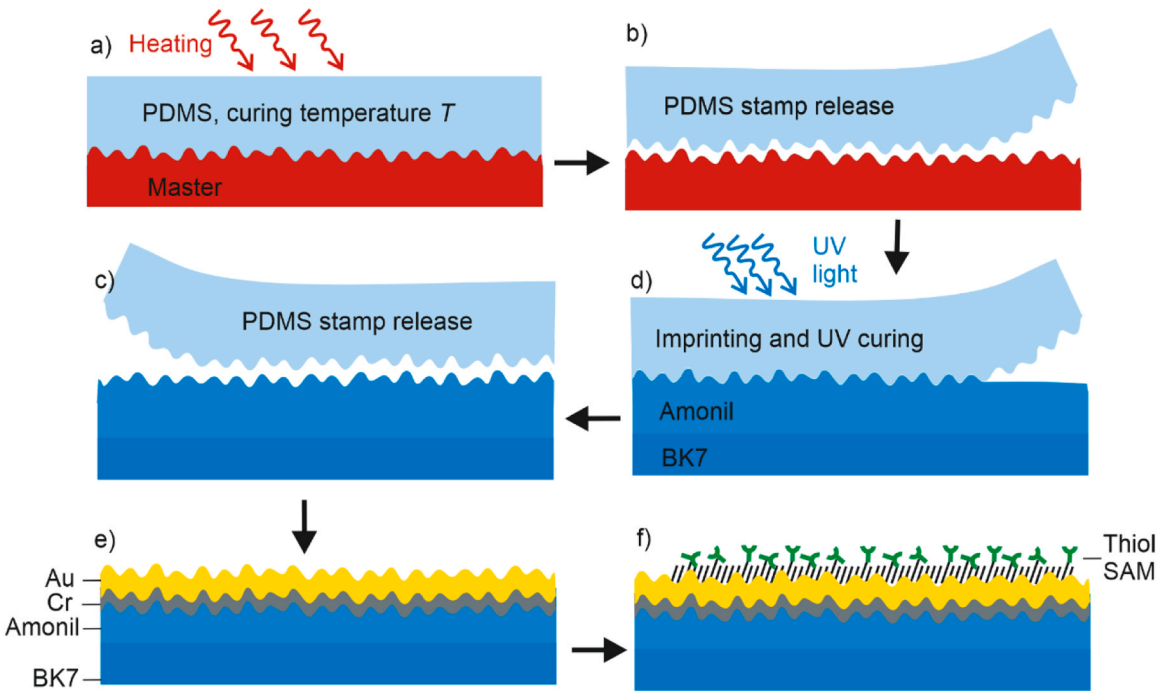

Fig. 1. Preparation of ACM-SPR sensor chip: a) casting of the PDMS stamp with a MPG corrugation, b) stamp release from the master structure, c) copying of the MPG to a UV-curable Amonil resin, d) stamp release from cured copy, e) coating with thin metal films, and f) modification with a biointerface.

2.5. Functionalization of sensor chips

Zwitterionic carboxybetaine (CB) and sulfobetaine (SB) thiols were synthesized based on the previously reported protocol [35]. Briefly, for the synthesis of SB thiol, 11-bromo-1-undecene was dissolved in THF then added to dimethylamine solution, and the reaction mixture was stirred at 50 °C for 16 h. The solvent was removed by rotovap under reduced pressure. 1 M NaOH was added to titrate the concentrated product, and the organic product was collected and extracted twice from diethyl ether. The organic solution was filtered through anhydrous sodium sulfate and finally concentrated by rotovap to give a clear brown oil of N,N-dimethyl-undec-10-enyl-amine. Then, N, N-dimethyl-undec-10-enyl-amine was dissolved in anhydrous acetone then added 1,3-propanesultone and stirred at *RT* for 2 days. The solution was added dropwise to acetone and recrystallized to get a white powder of 3-(N,N-dimethyl-undec-10-enyl-amino)-propane-1-sulfonic acid. 3-(N,N-dimethyl-undec-10-enyl-amino)-propane-1-sulfonic acid was mixed with methanol solution and thioacetic acid in an oxygen-free atmosphere. Then 2,2′-azo (2-methylpropionitrile) was added to the solution, and the solution was allowed to react for 36 h in a photoreactor at a wavelength of 365 nm under an oxygen-free environment. The resulting solution was added dropwise to anhydrous acetone and recrystallized to get a white powder. The powder was washed with a 1 M NaOH solution and neutralized using 1 M HCl solution. After precipitation in absolute ethanol, the white solid was removed by filtration. The solution was dried to give a white solid of 3-[(11-mercapto-undecyl)-N, N-dimethyl-amino]-propane-1-sulfonic acid (SB thiol).

For the synthesis of CB thiol, N,N-dimethyl-undec-10-enyl-amine was mixed with ethyl 4-bromobutyrate and acetonitrile and stirred at 50 ° C for 3 days. The solvent was removed by rotovap and the solution and was added dropwise to diethyl ether and stirred for 10 min. The supernatant was removed, and the product was purified twice to obtain a dark brown oil. The oil was mixed with methanol and thioacetic acid in a nitrogen atmosphere. Then 2,2′-azobis (2-methylpropionitrile) was added, and the mixture was allowed to react in a photoreactor at a wavelength of 365 nm for 36 h. The solvent was removed by rotovap under reduced pressure. The solution was added dropwise to diethyl ether for 10 min with stirring. The supernatant was removed to obtain yellow oil. The yellow oil product was dissolved in deionized water under nitrogen atmosphere and stirred for 5 min. Then 1 M aqueous sodium hydroxide was slowly added, followed by stirring for 3 h and neutralization using 1 M HCl solution. The product was dissolved in absolute ethanol and filtered to remove the white solid. The solution was then added dropwise to diethyl ether, and the supernatant was removed. After the final solution was concentrated by rotovap, bright yellow oil of CB thiol was obtained. ACM-SPR sensor chips with a thin Au film were rinsed with ethanol and treated with a UV ozone cleaner (from Jelight, USA) for 30 min. Immediately after the cleaning, they were immersed overnight in ethanolic solution with dissolved CB- and SB-thiols (0.2 mM and 0.8 mM, respectively) in order to form a self-assembled monolayer (SAM). After rinsing with ethanol, SAM-modified Au chips were dried under a stream of pressured nitrogen and stored in the dark under nitrogen atmosphere until use.

For calibration of the sensor response to surface mass density changes (Γ), a polyelectrolyte multilayer (PEM) assembly was conducted on the bare Au surface following a previously described protocol [14]. Briefly, solutions of PDADMAC and PSS at a concentration of 1 mg mL^{-1} were prepared in 100 mM KCl. PEM layers were assembled by alternating contacting of the sensor surface with PDADMAC and PSS solution for 15 minutes with rinsing steps in between. This sequence was repeated for a total of 8 layers, with PDADMAC as the initial layer.

2.6. Optical setup

Two optical setups were used for the readout of sensor response on the ACM-SPR sensor chip. Firstly, a simplified fiber optic readout with a non-collimated light beam was implemented with a polychromatic light beam emitted from a halogen light source (12 V, HL-2000-LL, Ocean Insight) launched to a Y-fiber optic splitter (400 μm core diameter, Thorlabs Inc.). The end of the one arm of fiber optic splitter was placed at the backside of the ACM-SPR sensor chip substrate (see Fig. 2**a**) and a polychromatic light beam cone emitted from the fiber irradiated the sensing spot. The beam was reflected from the Au-coated MPG structure and was collected by the same arm of the fiber optic splitter and

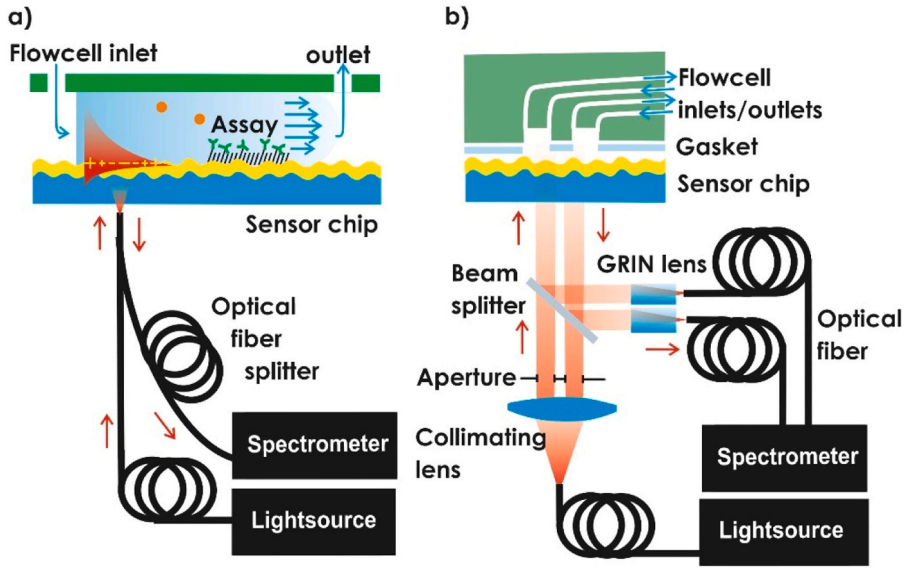

Fig. 2. Optical schematics of a) optical instrument for excitation and collection of probing light beam with a fiber coupler, and b) two-channel sensor configuration.

delivered *via* its second arm to a spectrometer (HR4000, Ocean Insight). The obtained wavelength spectra were normalized with a spectrum acquired from a reference flat Au surface. Reflectivity spectra were acquired with an integration time of 4 ms and averaging of 300 was used for reducing noise. For calibration of the ACM-SPR biosensor, a regular fiber optic SPR sensor with an optical fiber tip directly coated with a thin Au film was used [14]. The system was described previously and used the same optical fiber splitter, light source, and spectrometer as described above.

Secondly, a multichannel SPR spectrometer was adapted for the readout from two spots on the chip in parallel as schematically shown in Fig. 2**b**. A polychromatic beam emitted from a halogen lamp (HL2000 from Ocean Insight, USA) was coupled to an optical fiber (M25L01 from Thorlabs, UK) connected to a collimator with a lens focal distance of 50.0 mm. The beam passed through two square 3×3 mm^2 apertures in order to yield two parallel beams. These two spatially separated beams were made normally impinging at two sensing spots on the ACM-SPR sensor chip from the backside of the glass substrate. The reflected beams were separated from incident beams by a splitter (CCM1-BS014 from Thorlabs, UK) and they were directed towards two optical fibers (FT300EMT from Thorlabs, UK) with GRIN lens (GRINTECH, Germany) at their ends. Each beam coupled to the optical fiber was delivered to a spectrometer (FLAME-T from Ocean Optics, USA) and a custom software FunBIMS was used to acquire the raw wavelength spectra. Integration time of 25 ms and accumulation of 60 was applied. Against the ACM-SPR sensor chip surface, a flow-cell was clamped in order to transport analyzed liquid samples to the sensing spots. It consisted of a module printed using stereolithography (Prusa Sl1s, resin Prusa green transparent). After printing, the part was rinsed thoroughly with isopropyl alcohol, dried with a nitrogen stream, and post-cured with UV light. Input and output channels of the two flow chambers were connected with input and output tubing (Tygon LMT-55, Ismatek, Germany). These flow chambers were defined by a PDMS gasket, and their volume was 5.6 μL. The gasket was cut from a PDMS sheet with a thickness of approx. 0.34 mm by using a plotter (Silhouette Cameo® 4 from Silhouette America, USA). Liquid samples were flowed over the sensor chip surface at *RT* using a peristaltic pump (Ismatek, Germany) at a flow rate of 30 μL min^{-1}, while washing steps were performed at a higher flow rate of 60 μL min^{-1}.

As reference optical system, a prism-based ATR SPR biosensor with Kretschmann configuration was used. It was assembled from the same components as the previous system, but the beam splitter was replaced by an optical prism (made from LASF9 glass, 60°) to which a sensor chip, with a flat 2 nm Ti and 50 nm Au thick films (prepared by L.E.T. Optomechanika, Czech Republic) was optically matched with immersion oil (from Cargille, USA). The prism and output optical fibers were mounted on a rotation stage that allowed controlling the angle of incidence θ.

2.7. Data processing

Raw reflectivity spectra acquired from ACM-SPR sensor chip area carrying the MPG were normalized with those measured from a reference flat Au-coated surface and recorded as a time series. They were then processed by in house written Python scripts. To obtain sensorgrams from the recorded spectra, for every time step the average intensity $\overline{R}(\lambda_i)$ was calculated for wavelengths of λ_L and λ_S (see discussion of measured spectra in the results part). An averaging over spectral bands centered at λ_L and λ_S was applied to reduce noise (100 pixels corresponding to a width of the spectral bands of about 8 nm). The averaged intensities are then divided to calculate the ACM-SPR signal $\overline{R}(\lambda_L)/\overline{R}(\lambda_S)$ and exported as time series. In reference SPR biosensor configuration with prism coupler ATR method, reflectivity spectra were $R(\lambda)$ measured for transverse magnetic polarization normalized with transverse electric polarization with an angle of incidence set to about 42°. The sensor output was defined as resonant wavelength λ_{SPR}, which was determined by fitting of SPR dips with a polynomial function.

3. Results

The implementation of the proposed ACM-SPR biosensor was carried out with two optical configurations enabling spectral interrogation of resonantly excited PSPs on the sensor surface bearing MPG. In the first configuration shown in Fig. 2**a**, a multimode optical fiber was used for the backside excitation of PSPs. In this sensor design, a non-collimated polychromatic optical beam probed the sensor surface by positioning an optical fiber tip directly below the glass substrate supporting the sensor chip. The same fiber was also used for collecting the reflected beam from the MPG structure and its delivery to a spectrometer. In the second configuration, we implemented a two-channel configuration, where two parallel collimated polychromatic beams were made impinging at two spatially distinct sensing spots. These beams reflected from the surface with MPG and were delivered to two spectrometers. As

discussed further, the sensor chips with metallic MPGs structure were optimized for the readout of minute refractive index changes and the effect of the beam divergence (that smears the resonance in regular grating-coupled SPR) was investigated. Afterwards, the application of the developed sensor platforms with the ACM-SPR for the monitoring of affinity biomolecular interactions is demonstrated. The performance of the sensor is compared by carrying out a readout of the same assay by conventionally used SPR biosensor with Kretschmann geometry of ATR that uses the same optical components.

The ACM-SPR relies on MPG structure that is designed for diffraction-based cross coupling between the PSP modes on opposite interfaces as detailly discussed in our previous work [26]. Briefly, the MPG structure is composed of two overlayed sinusoidal corrugations with long-period (Λ_1) and short-period (Λ_2) components. These corrugations are prepared in a crossed (orthogonally oriented) pattern and it is conformally coated with a thin Au film. The corrugation Λ_1 serves for resonant excitation of surface plasmon modes PSP_i at the inner (substrate) side of the thin Au film *via* first-order diffraction phase-matching. Their cross-coupling through the thin Au film to the surface plasmons PSP_o at the outer (sensor) side is achieved by the short-period corrugation Λ_2. Spectral range where the optical excitation with a normally incident optical beam occurs and the efficiency of the coupling across the thin Au film can be tuned by the design of the periods and respective corrugation amplitudes.

3.1. Tuning of sensor chips for ACM-SPR

Relief MPG structure was prepared by using a PDMS working stamp and UV-nanoimprint lithography that was followed by the coating with a thin Au layer (see Fig. 1). The corrugation profile carried by the master structure (periods Λ_1=456 nm and Λ_2= 239 nm) can be modified upon the replication process and herein we investigated its finetuning for optimum performance for the ACM-SPR. Topography of the imprinted MPG copies after their coating with an Au film was measured with AFM as shown in Fig. 3**a**. AFM micrographs were analyzed with fast-Fourier transformation (FFT) to determine the periods and amplitudes of MPG components as presented in Fig. 3**b**. Interestingly, these data show that the curing condition of the PDMS stamp (performed at room temperature *RT*=20–22°C and elevated temperature of 60°C) allows for shifting the periods Λ_1 and Λ_2 without substantially affecting the modulation amplitudes. When the PDMS stamp was cured at *RT*, periods of Λ_1 and Λ_2 of the copy matched the values measured for the master. The curing at elevated temperature of 60°C resulted in shorter periods of the copied structure due to the thermal contraction of the PDMS stamp used for the imprinting at *RT*. A reduction of the periods $\Delta\Lambda_1 = -8$ nm and $\Delta\Lambda_2 = -7$ nm was evaluated from the data presented in Fig. 3**b**. These results demonstrate that the UV-NIL replication process can be efficiently controlled to fine-tuning the MPG structure without the necessity of fabricating multiple master substrates.

The impact of tuning the MPG corrugation periods Λ_1 and Λ_2 to its plasmonic properties is assessed by measuring reflectivity spectra $R(\lambda)$ with a collimated normally incident beam ($\theta = 0$). As can be seen in Fig. 3**c**, the excitation of cross-coupled PSP modes exhibit itself as two overlapping Lorentzian dips with minima located at shorter wavelength λ_S (close to 700 nm) and longer wavelength λ_L (in vicinity to 740 nm). The shortening of periods Λ_1 and Λ_2 by curing the PDMS stamp at elevated temperature leads to a weak blue shift of the resonant wavelengths ($\Delta\lambda_S = -1$ nm and $\Delta\lambda_L = -4.5$ nm) and strongly pronounced changes in the coupling strength [represented by the intensities $R(\lambda_S)$ and $R(\lambda_L)$ at respective minima]. In particular, the changes in coupling strength evolves in opposite sense at λ_S and λ_L. The depth of the dip at λ_S increases while that at λ_L decreases when shortening the periods Λ_1 and Λ_2, indicating an anti-crossing nature of the involved SPR resonances on the used plasmonic MPG.

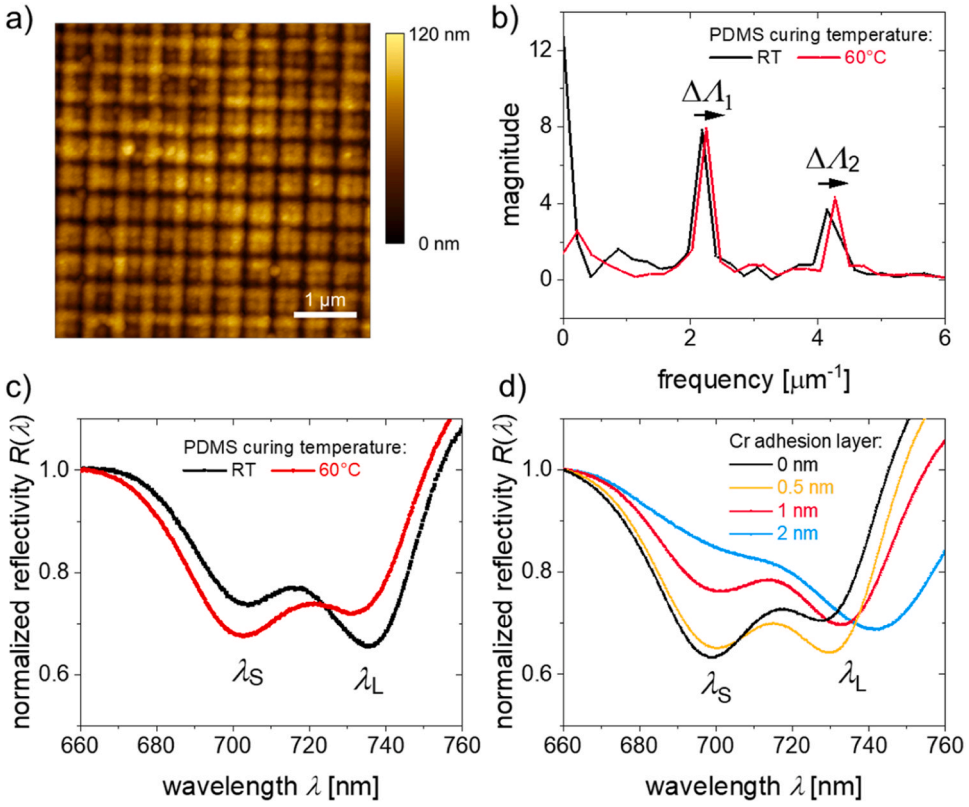

Fig. 3. a) AFM characterization of MPG topography with b) respective FFT analysis. Comparison of SPR spectra measured for sensor chip with c) tuned MPG periods Λ_1 and Λ_2 upon the imprinting step and d) for varied thickness of Cr layer $d_{Cr}$when the PDMS stamp curing temperature was of 60 °C. The sensor chip was contacted with water n=1.33 and reflectivity spectra were measured with normally incident collimated beam ($\theta = 0$).

Besides the MPG topography, also the metallic thin film structure affects the optical excitation of PSP modes. Strong adhesion of the Au layer to the substrate is essential for maintaining the integrity of the SPR sensor chip over time, a crucial aspect for substrates undergoing further microfabrication steps needed in more complex sensor architectures and when utilized for surface modification in solvents. Even though the chemical composition of the nanoimprint resist (Amonil) promotes the adhesion of Au, it was not sufficient and delamination or cracking of the Au film was observed if the sensor chips are exposed to solvents and/or mechanical stress (see Fig. S1). It is very well established that a thin Cr layer, typically 2 nm in thickness, significantly improves the adhesion of Au to an oxide substrate. However, Cr is a very poor plasmonic material due to its strong optical damping, which is a drawback for the backside excitation of PSPs using the investigated MPG structure. The resulting reflectivity spectra $R(\lambda)$ obtained from sensor chips with a Cr adhesion layer thickness between $d_{Cr} = 0$ and 2 nm and d_{Au}=50 nm are shown in Fig. 3**d**. While a thickness of $d_{Cr} = 0.5$ nm showed only minimal improvement in Au adhesion (Fig. S1), a 2 nm thick Cr layer almost completely quenched the cross-coupling (by broadening the spectra and shifting the phase-matching condition to a longer wavelength spectral region). A thickness of $d_{Cr} = 1$ nm of the Cr adhesion layer appeared to be an optimum compromise between enhanced Au adhesion and increased damping. In addition, it allowed for balancing the coupling strength to two cross-coupled bands with $R(\lambda_S) \sim R(\lambda_L)$.

3.2. Angular dependence of AMT-SPR

The optical mechanism of the cross-coupling was detailly discussed in our previous work [26] and it was attributed to opening of a bandgap in the dispersion relation of surface plasmons travelling at the inner (PSP_i) and outer (PSP_o) interfaces and spectral alignment of their branches. The spectral window, where these modes are excited, is controlled by the thin metal film corrugation Λ_1 and refractive indices of the (glass) substrate and (sensed biointerface) superstrate. In addition, an important role plays the width of the bandgaps that is tuned by the amplitude of Λ_2. It is worth noting that the design of the MPG allows to implement the cross-coupling mechanism only for a certain spectral window and refractive index range of the medium contacted with its surface. As investigated further, modulating the refractive index n detunes the spectral position of the surface plasmon bandgaps and it is manifested as two reflectivity dips with gradually swapping depth rather than spectral shift typically used in SPR biosensors.

The anti-crossing character of the resonant excitation of PSP modes at the surface of the developed MPG sensor chip was investigated by the measurement of angular and wavelength dependence of reflectivity $R(\lambda,\theta)$. These spectra were measured for backside coupling to PSPs traveling along the MPG structure contacted with water (refractive index n=1.330) and 50 % ethylene glycol (refractive index n=1.382). As Fig. 4**a,b** shows, diffraction of PSPs manifests itself as V-shaped dispersion relation for the angles $\theta > 10$ °. This behavior is similar to diffraction coupling to PSP on regular periodically corrugated gratings and can be attributed to the first order diffraction phase-matching with PSPs at the inner surface of the Au film (see schematics in Fig. 4**d**) *via* the MPG component Λ_1. However, the measured spectra show a different, more complex dependence of $R(\lambda,\theta)$ at smaller angles $\theta < 10$ °. A gap appears in the wavelength range between 750 and 790 nm with an anti-crossing coupling to PSPs in the short wavelength dispersion branch located in wavelength region 700 – 740 nm. The short wavelength branch exhibits two narrow resonances centered at wavelengths λ_S and λ_L, which weakly shift and swap their coupling strength when increasing refractive index n on the top of the MPG surface (Fig. 4**c**). Due to this character, we use in this paper the term anti-crossing of surface plasmon branches referring to other plasmonic systems with qualitatively similar behavior [36]. In line with the previous observations in Fig. 3,

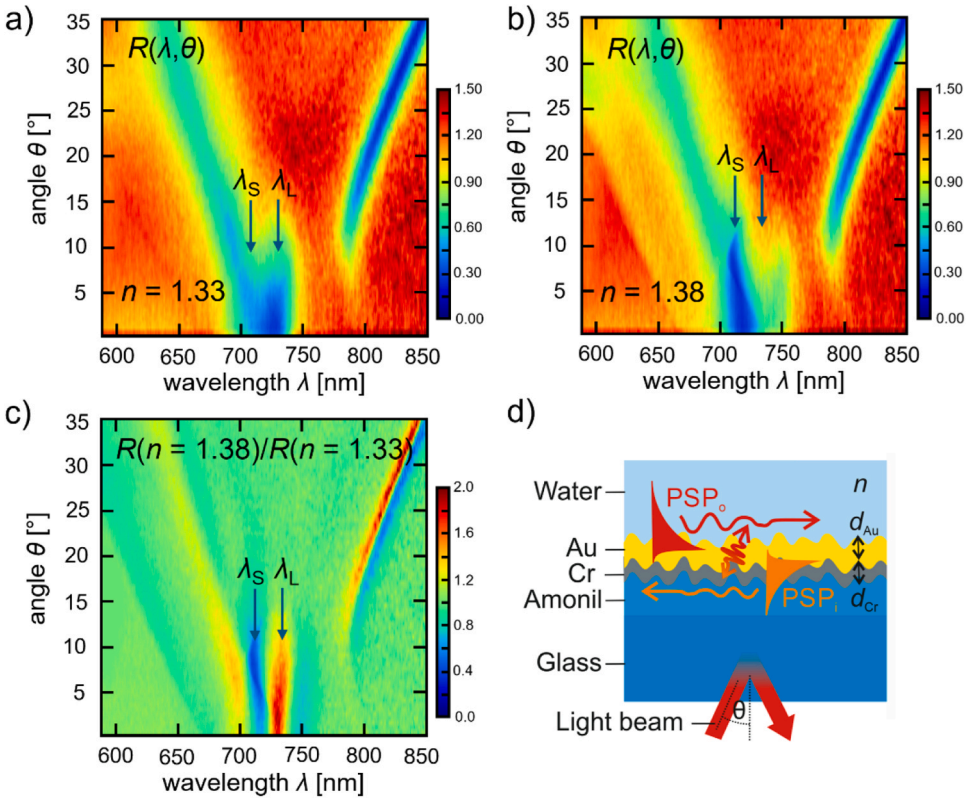

Fig. 4. Reflectivity dependence on angle of incidence and wavelength $R(\lambda,\theta)$ for MPG structure contacted with a) water n=1.330 and b) with 50 % ethylene glycol n=1.382. c) Ratio of the reflectivity spectra $R(n = 1.38)/R(n = 1.33)$. d) Schematics of the used geometry with a light beam impinging on the surface with MPG facilitating a backside excitation of PSP at the outer interface contacted with a liquid sample.

increasing the refractive index n leads to an enhanced coupling strength at the short wavelength resonance λ_S and reduced coupling strength at λ_L. Importantly, this interaction is weakly dependent on the angle of incidence θ in the range 0–10 °, which corresponds to the numerical aperture of 0.17 (Fig. 4**c**).

3.3. Signal analysis and calibration

The observed changes in SPR reflectivity spectra were utilized for the monitoring of molecular binding-induced refractive index changes with optimized signal-to-noise ratio. In this study, the fiber optic setup was used for the excitation of PSPs by using a diverging light cone emitted from an optical fiber end positioned below the MPG sensor chip. Firstly, a centroid method was tested to quantify changes in the acquired SPR spectra $R(\lambda)$ similar to the previous study [26]. Briefly, a wavelength range $\lambda_{N1} - \lambda_{N2}$ and a threshold R_t were set (Fig. S2a) for determining the centroid wavelength from discrete reflectivity values acquired from the spectrometer detector pixels according to Eq. S1 [30]. The outcome of this approach was strongly changing with small variations of parameters λ_{N1}, λ_{N2}, and R_t, which severely hindered the reproducibility of the acquired data. The reason is that the centroid responds in opposite manner to the coupling strength changes and to weak spectral shifts of the bands at λ_S and λ_L. Therefore, another more robust approach was pursed based on PSP mode anti-crossing modulation – ACM. There was exploited the opposite response of reflectivity at λ_S and λ_L to a change of refractive index n on the MPG. In the proposed ACM-SPR method, the minimum intensity of the short wavelength dip $R(\lambda_S)$ and longer wavelength dip $R(\lambda_L)$ were determined. In order to reduce the noise, intensity values in the vicinity to the minima positions were averaged over a range of wavelengths, with an optimum of averaging 100 spectral points (see SI). The SPR output signal was defined as ratio between the averaged intensity values $\overline{R}(\lambda_L)/\overline{R}(\lambda_S)$ (Fig. S2b).

The ACM-SPR response was further calibrated to determine changes in surface mass density Γ associated with molecular binding events. Therefore, PEMs were assembled using a layer-by-layer approach by alternating exposure of the sensor surface to a solution with positively charged PDADMAC and negatively charged PSS polymers (Fig. 5**a**). Following the deposition of each layer, the reflectivity spectra and respective ACM-SPR response $\overline{R}(\lambda_L)/\overline{R}(\lambda_S)$ was recorded, see Fig. 5**b**. The same procedure was replicated with a reference fiber optic FO-SPR sensor with the known SPR response per PEM layer [14] to establishing a direct relationship presented in Fig. 5**c**. The obtained linear fit yielded a correlation factor of $1 \bullet 10^{-4}$ cm^2 ng^{-1} (R^2 of 0.99) for optimized ACM-SPR chips (fabricated with PDMS working stamps cured at elevated temperature and with a Cr adhesion layer thickness d_{Cr} of 1 nm).

3.4. Development of CSPG4 immunoassay

ACM-SPR sensor chips were employed for the characterizing of sandwich immunoassays for chondroitin sulfate proteoglycan 4 (CSPG4), which has been identified as a melanoma cancer biomarker and potential candidate for immunotherapy [37]. The prepared sensor chips were loaded to a dual-channel optical reader system, where the probing of spatially separated sensing spots was performed in parallel with two collimated polychromatic beams (see Fig. 2**b**). As illustrated in Fig. 6**a**, sensor chips with an Au layer-coated MPG structure were modified with a mixed thiol SAM bearing antifouling zwitterionic carboxybetaine (CB) and sulfobetaine (SB) headgroups. The composition of CB and SB was set to the ratio 1:4. The carboxyl group in CB thiol served for the covalent attachment of protein molecules *via* amine coupling and a SB carpet was used to repel nonspecific interactions with the surface. Two monoclonal antibodies, Ep2 and Ep3, were tested for affinity binding to the CSPG4 analyte. The herein tested format includes affinity binding of CSPG4 present in the liquid sample to the sensor surface with anchored antibody (see Fig. 6**a, channel A**) or *vice versa* (see Fig. 6**a, channel B**), conducted simultaneously on the same sensor chip.

The measured sensor response is presented in Fig. 6**b**. The surface of both channels A and B was firstly rinsed with water and PBS, and then carboxylic moieties of the CBs groups were activated by a freshly prepared aqueous mixture of EDC (0.4 M) and NHS (0.1 M) for 10 min. Afterwards, the Ep3 antibody, dissolved in PBS (125 nM), was flowed over the sensor surface of channel A for 10 min (see the upper part of Fig. 6**b**). The AMC-SPR sensor response gradually increased due to the covalent coupling of Ep3 to the activated CB groups. Based on the sensor response, surface mass density of the coupled Ep3 antibody of $\Gamma = 141 \pm 5$ ng cm^{-2} was determined, taking the above-established calibration factor (Fig. 5**c**) into account. By injecting ethanolamine, the excess of the activated CB groups (not reacted with the antibody) were passivated. For the affinity interaction study, PBS was replaced with the working buffer PBS-Tween-BSA to block the surface and further prevent nonspecific binding. CSPG4 (125 nM) was allowed to interact with the Ep3 in two steps with a duration of 20 min. After washing with working buffer PBS-Tween-BSA, the ACM-SPR sensor response for the CSPG4 binding corresponds to a Γ of 305 ± 11 ng cm^{-2} for the bound CSPG4. Finally, the Ep2 dissolved in the working buffer (125 nM) was introduced to the sensor and flowed over the sensor surface for 18 min. The measured response indicates, that Ep2 can bind to the protein on a

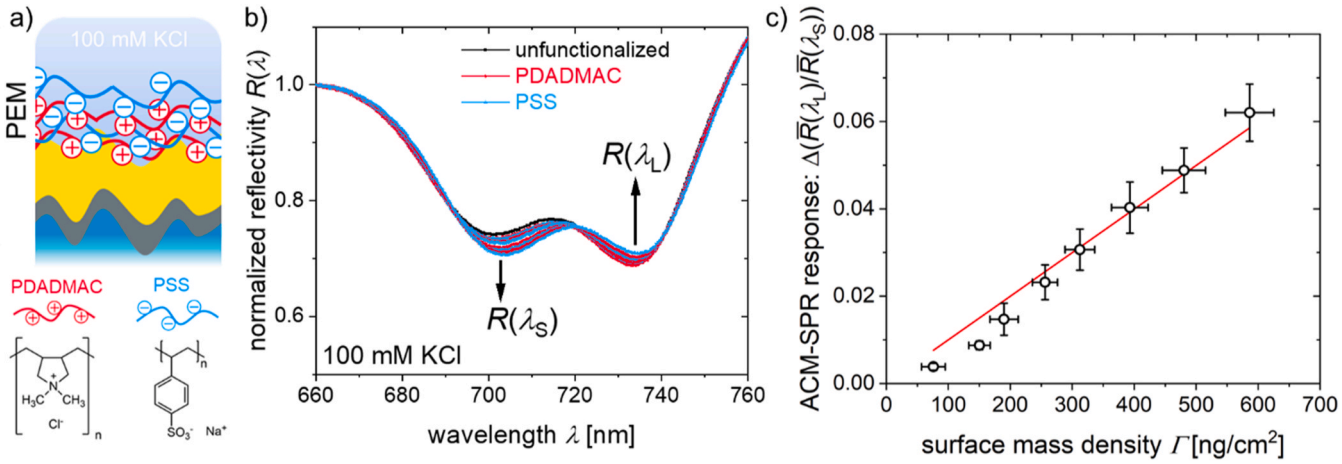

Fig. 5. a) Schematic representation of the PEM LbL assembly on the sensor surface. b) Measured SPR spectra changes upon LbL deposition of PSS and PDADMAC polymer multilayer with c) dependence of the sensor output on Γ (for the ACM-SPR sensor chip prepared from a PDMS master casted at elevated temperature of 60 °C and using a 1 nm thick Cr adhesion layer). The red line corresponds to the linear fit.

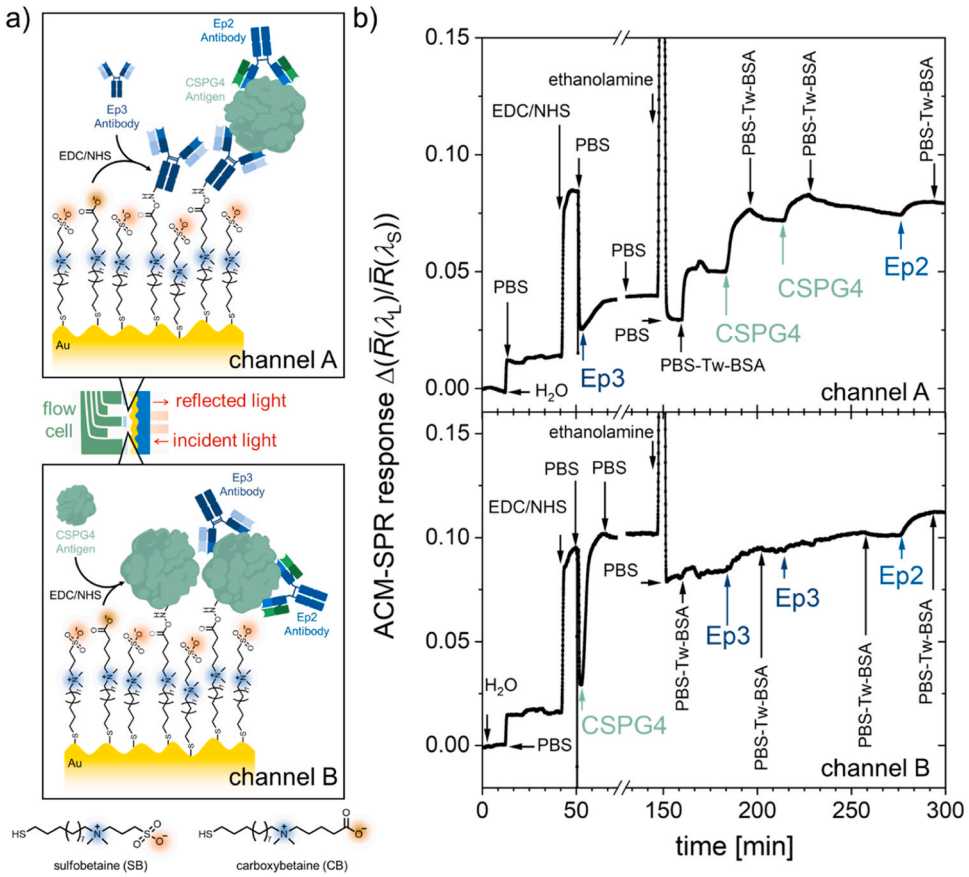

Fig. 6. a) Schematics of the used amine coupling in conjunction with mixed thiol SAM (carboxybetaine (CB) and sulfobetaine (SB)) on the Au surface for the immobilization of antibody Ep3 (channel A) and antigen CSPG4 (channel B). b) SPR-ACM sensorgram of functionalization and affinity interaction between CSPG4 and Ep2,3 antibodies.

different specific region compared to the surface-immobilized Ep3. This possibility for a sandwich assay using Ep2 and Ep3 antibodies was further confirmed by an ELISA test (see SI).

In the second channel B (bottom part of Fig. 6**b**), CSPG4 dissolved in PBS (125 nM) was introduced to the surface for 10 min. The AMC-SPR sensor response rapidly increased owing to the covalent coupling with the CB groups. The surface was passivated by injecting ethanolamine, washing off the weakly bound molecules of the sensor surface. The overall larger ACM-SPR response for the CSPG4 coupling to the activated SAM compared to the Ep3 antibody coupling (see channel A) can be ascribed to the difference in molecular weight of CSPG4 (250 kDa) compared to IgG antibodies (150 kDa). The surface-bound CSPG4 resulted in surface mass density of $\Gamma = 704 \pm 26$ ng cm^{-2}. Then, PBS was replaced with the working buffer. Ep3 (125 nM) was injected to interact with the CSPG4 in two steps with a duration of 20 min. After washing with the working buffer, the ACM-SPR sensor response to Ep3 binding corresponds to a Γ of 176 ± 7 ng cm^{-2}. Finally, the Ep2, dissolved in the working buffer (125 nM), was flowed over the sensor surface for 18 min. Similarly to channel A, the measured response in channel B shows that Ep2 can recognize the protein CSPG4 from its

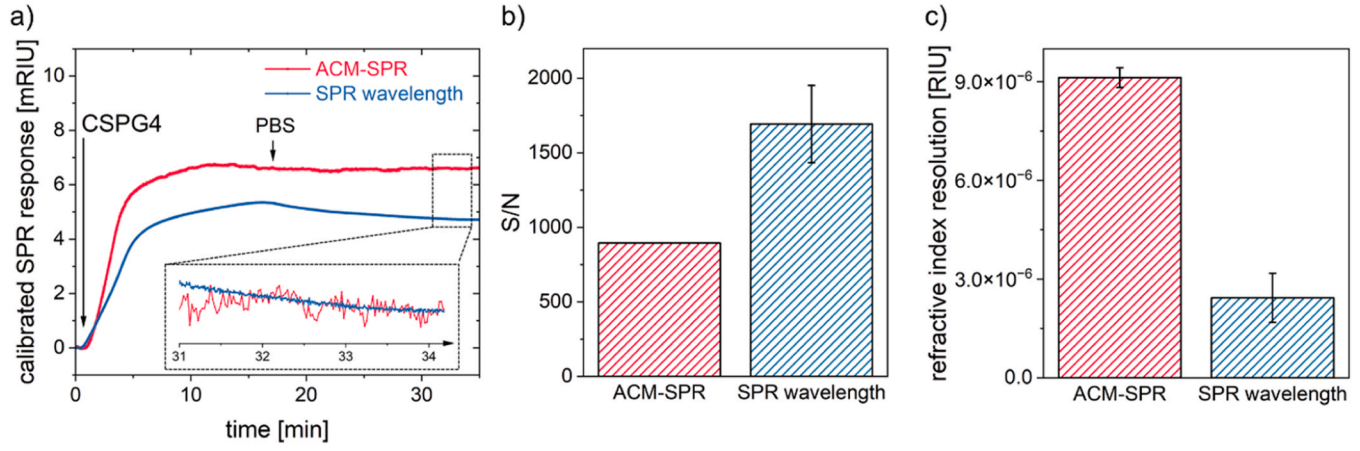

Fig. 7. Comparison of SPR-ACM and regular SPR biosensor with spectral interrogation for a) the signal of CSPG4 coupling to the EDC/NHS activated SAM (inset shows a zoom-in of the noise level), b) the obtained signal-to-noise (S/N) ratio for the CSPG4 coupling, and c) the refractive index resolution.

specific paratope region.

The accuracy of the reported ACM-SPR approach was compared with the regular implementation of an ATR-based biosensor with wavelength interrogation of SPR. The ATR-based SPR instrument was configured to probe a flat Au sensor surface with resonantly excited PSPs at a similar wavelength of $\lambda_{SPR} = 670$ nm. The sensor output was measured with the same optical components including light source, input and output optical fibers, spectrometers, and microfluidic device. Fig. 7**a** compares the sensor responses for the covalent coupling of the CSPG4 protein to the mixed thiol SAM. Both sensorgrams show a similar profile of the CSPG4 binding kinetics, with a slightly higher overall signal for the calibrated ACM-SPR response. However, the higher noise level obtained for the ACM-SPR approach results in a reduced, yet still comparable, signal-to-noise (S/N) ratio for the CSPG4 coupling compared to the regular, ATR-based biosensor with wavelength interrogation of SPR (Fig. 7**b**). Even though the regular ATR SPR provided slightly better refractive index resolution (Fig. 7**c**), the ACM-SPR approach presents similar performance while allowing the use of simplified optical components. The determined refractive index resolution of $3–9\times10^{-6}$ RIU is in the range of other regular grating – based SPR biosensors reported in literature [19]. Thus, we believe that the developed sensor chip holds great potential for a broad range of sensing applications, particularly in the context of point-of-care diagnostics.

4. Conclusions

In summary, we have devised a versatile approach to direct label-free biosensing with wavelength interrogation of SPR based on tailored multiperiodic plasmonic grating - MPG - supporting cross-coupled PSP modes. It allows for diffraction-based backside excitation of PSPs and an implementation with fiber optic SPR system and in a configuration compatible with conventional ATR biosensor is demonstrated. In comparison with regular grating-coupled SPR biosensors, the necessity of probing of the sensor surface with a collimated beam passing through the analyzed sample is avoided. In addition, we report on a new approach to evaluation of SPR spectra changes which can be in future implemented without the need of spectrometers. The reported anti-crossing modulation of SPR, which relies on monitoring of intensity ratio of two neighboring absorption bands in the wavelength spectrum, can be carried out based on two narrow bandpass filters. Despite the simplicity, the ACM-SPR offers similar accuracy in terms of refractive index resolution as regular SPR biosensors. The implementation of ACM-SPR is discussed in terms of fine-tuning the MPG structure, its sensitivity to bulk refractive index changes as well as surface mass density variations. The potential of ACM-SPR for biomolecular affinity interaction studies is demonstrated through an experiment where the implementation of sandwich CSPG4 immunoassay is investigated in connection to self-assembled biointerfaces with zwitterionic headgroups. The obtained results revealed a possibility to form sandwich with the use of monoclonal antibodies Ep2 and Ep3 and allowed for quantifying the molecular binding ratios.

CRediT authorship contribution statement

Jiri Perutka: Writing – original draft, Investigation. **Patrizio Giacomini:** Writing – original draft, Methodology. **Christoph Kleber:** Funding acquisition. **Kamil Onder:** Funding acquisition. **Chun-Jen Huang:** Writing – original draft, Methodology, Investigation, Funding acquisition, Data curation. **Dario Cattozzo Mor:** Writing – original draft, Methodology, Investigation. **Paolo Samorì:** Funding acquisition. **Roger Hasler:** Writing – original draft, Validation, Investigation, Data curation. **Gizem Aktug:** Writing – original draft, Methodology, Investigation. **Jakub Dostalek:** Writing – original draft, Supervision, Funding acquisition, Conceptualization. **Van Truc Vu:** Methodology, Investigation. **Stefan Fossati:** Writing – original draft, Methodology, Investigation. **Elena Riccardia:** Investigation. **Elena Giordani:** Writing – original draft, Methodology. **Adrián Tamayo:** Methodology.

Declaration of Competing Interest

The authors declare that they have no known competing financial interests or personal relationships that could have appeared to influence the work reported in this paper.

Data Availability

The data that support the findings of this study are openly available in Zenodo (10.5281/zenodo.11504015).

Acknowledgements

D.C.M., G.A., and J.D. were supported by Czech Science Fund (GACR) project APLOMA (22-30456J). V.T and C.J.H acquired support by the National Science and Technology Council, Taiwan (NSTC 111-2628-E-008-003-MY3, 111–2923-E-008–004-MY3, and 112-2221-E-008-007-MY3). S.F., G.A., J.D., J.R., K.O., P.G. were supported by European Union's European Innovation Council (EIC) under Horizon Europe program project Versilib (grant agreement 101046217). D.C.M and G.A. also acknowledge support from the Charles University by SVV–2023–260716. JD and SF are grateful for the support from Operational Programme Johannes Amos Comenius financed by European Structural and Investment Funds and the Czech Ministry of Education, Youth, and Sports (Project No. SENDISO-CZ.02.01.01/00/22_008/0004596). C.K., R.H. thank the office of the Federal Government of Lower Austria, K3-Group - Culture, Science and Education, for their financial support as part of the project "Responsive Wound Dressing". P. S. acknowledges financial support through the ANR through the Interdisciplinary Thematic Institute SysChem via the IdEx Unistra (ANR-10-IDEX-0002) within the program Investissement d'Avenir and the Foundation Jean-Marie Lehn. R.H. thanks Dr. Juan Allegretto for helpful scientific discussions and support with the microscope images of the substrates.

Appendix A. Supporting information

Supplementary data associated with this article can be found in the online version at doi:10.1016/j.snb.2024.136163.

References

[1] J.-F. Masson, Surface plasmon resonance clinical biosensors for medical diagnostics, ACS Sens 2 (2017) 16–30, https://doi.org/10.1021/acssensors.6b00763.
[2] M. Herrera-Domínguez, G. Morales-Luna, J. Mahlknecht, Q. Cheng, I. Aguilar-Hernández, N. Ornelas-Soto, Optical biosensors and their applications for the detection of water pollutants, Biosensors 13 (2023) 370, https://doi.org/10.3390/bios13030370.
[3] J. Zhou, Q. Qi, C. Wang, Y. Qian, G. Liu, Y. Wang, L. Fu, Surface plasmon resonance (SPR) biosensors for food allergen detection in food matrices, Biosens. Bioelectron. 142 (2019) 111449, https://doi.org/10.1016/j.bios.2019.111449.
[4] T. Brulé, G. Granger, N. Bukar, C. Deschênes-Rancourt, T. Havard, A.R. Schmitzer, R. Martel, J.-F. Masson, A field-deployed surface plasmon resonance (SPR) sensor for RDX quantification in environmental waters, Analyst 142 (2017) 2161–2168, https://doi.org/10.1039/C7AN00216E.
[5] W. Na, M. Kang, D. Jang, S. Shin, Miniaturized surface plasmon resonance biosensor with vacuum-driven hydrodynamic focusing, Sens. Actuators B: Chem. 254 (2018) 64–71, https://doi.org/10.1016/j.snb.2017.07.041.
[6] J. Zhang, I. Khan, Q. Zhang, X. Liu, J. Dostalek, B. Liedberg, Y. Wang, Lipopolysaccharides detection on a grating-coupled surface plasmon resonance smartphone biosensor, Biosens. Bioelectron. 99 (2018) 312–317, https://doi.org/10.1016/j.bios.2017.07.048.
[7] G.P. Singh, N. Sardana, Smartphone-based surface plasmon resonance sensors: a review, Plasmonics 17 (2022) 1869–1888, https://doi.org/10.1007/s11468-022-01672-1.
[8] D. Harpaz, B. Koh, R.S. Marks, R.C.S. Seet, I. Abdulhalim, A.I.Y. Tok, Point-of-care surface plasmon resonance biosensor for stroke biomarkers NT-proBNP and S100β using a functionalized gold chip with specific antibody, Sensors 19 (2019) 2533, https://doi.org/10.3390/s19112533.

[9] I. Víšová, M. Houska, H. Vaisocherová-Lísalová, Biorecognition antifouling coatings in complex biological fluids: a review of functionalization aspects, Analyst 147 (2022) 2597–2614, https://doi.org/10.1039/D2AN00436D.
[10] R. D'Agata, N. Bellassai, V. Jungbluth, G. Spoto, Recent advances in antifouling materials for surface plasmon resonance biosensing in clinical diagnostics and food safety, Polymers 13 (2021) 1929, https://doi.org/10.3390/polym13121929.
[11] D. Geilfuss, R. Boukherroub, J. Dostalek, W. Knoll, J.-F. Masson, A.J. Baeumner, S. Szunerits, Can classical surface plasmon resonance advance via the coupling to other analytical approaches? Front. Anal. Sci. 2 (2022) 1091869 https://doi.org/10.3389/frans.2022.1091869.
[12] T. Chen, J. Xin, S.J. Chang, C. Chen, J. Liu, Surface Plasmon Resonance (SPR) combined technology: a powerful tool for investigating interface phenomena, Adv. Mater. Inter 10 (2023) 2202202, https://doi.org/10.1002/admi.202202202.
[13] P. Aspermair, U. Ramach, C. Reiner-Rozman, S. Fossati, B. Lechner, S.E. Moya, O. Azzaroni, J. Dostalek, S. Szunerits, W. Knoll, J. Bintinger, Dual monitoring of surface reactions in real time by combined surface-plasmon resonance and field-effect transistor interrogation, J. Am. Chem. Soc. 142 (2020) 11709–11716, https://doi.org/10.1021/jacs.9b11835.
[14] R. Hasler, C. Reiner-Rozman, S. Fossati, P. Aspermair, J. Dostalek, S. Lee, M. Ibáñez, J. Bintinger, W. Knoll, Field-effect transistor with a plasmonic fiber optic gate electrode as a multivariable biosensor device, ACS Sens 7 (2022) 504–512, https://doi.org/10.1021/acssensors.1c02313.
[15] J.A. Ribeiro, M.G.F. Sales, C.M. Pereira, Electrochemistry combined-surface plasmon resonance biosensors: a review, TrAC Trends Anal. Chem. 157 (2022) 116766, https://doi.org/10.1016/j.trac.2022.116766.
[16] Y. Zong, F. Xu, X. Su, W. Knoll, Quartz crystal microbalance with integrated surface plasmon grating coupler, Anal. Chem. 80 (2008) 5246–5250, https://doi.org/10.1021/ac800393d.
[17] C. Song, J. Zhang, X. Jiang, H. Gan, Y. Zhu, Q. Peng, X. Fang, Y. Guo, L. Wang, SPR/SERS dual-mode plasmonic biosensor via catalytic hairpin assembly-induced AuNP network, Biosens. Bioelectron. 190 (2021) 113376, https://doi.org/10.1016/j.bios.2021.113376.
[18] B. Liedberg, C. Nylander, I. Lundström, Biosensing with surface plasmon resonance — how it all started, Biosens. Bioelectron. 10 (1995) i–ix, https://doi.org/10.1016/0956-5663(95)96965-2.
[19] C. Boozer, Q. Yu, S. Chen, C.-Y. Lee, J. Homola, S.S. Yee, S. Jiang, Surface functionalization for self-referencing surface plasmon resonance (SPR) biosensors by multi-step self-assembly, Sens. Actuators B: Chem. 90 (2003) 22–30, https://doi.org/10.1016/S0925-4005(03)00017-0.
[20] D. Harpaz, B. Koh, R.C.S. Seet, I. Abdulhalim, A.I.Y. Tok, Functionalized silicon dioxide self-referenced plasmonic chip as point-of-care biosensor for stroke biomarkers NT-proBNP and S100β, Talanta 212 (2020) 120792 https://doi.org/10.1016/j.talanta.2020.120792.
[21] F. Delport, J. Pollet, K. Janssen, B. Verbruggen, K. Knez, D. Spasic, J. Lammertyn, Real-time monitoring of DNA hybridization and melting processes using a fiber optic sensor, Nanotechnology 23 (2012) 065503, https://doi.org/10.1088/0957-4484/23/6/065503.
[22] J. Dostálek, J. Homola, M. Miler, Rich information format surface plasmon resonance biosensor based on array of diffraction gratings, Sens. Actuators B: Chem. 107 (2005) 154–161, https://doi.org/10.1016/j.snb.2004.08.033.
[23] M. Abutoama, I. Abdulhalim, Self-referenced biosensor based on thin dielectric grating combined with thin metal film, Opt. Express 23 (2015) 28667, https://doi.org/10.1364/OE.23.028667.
[24] J. Dostálek, P. Adam, P. Kvasnička, O. Telezhnikova, J. Homola, Spectroscopy of Bragg-scattered surface plasmons for characterization of thin biomolecular films, Opt. Lett. 32 (2007) 2903, https://doi.org/10.1364/OL.32.002903.
[25] B. Spackova, P. Wrobel, M. Bockova, J. Homola, Optical biosensors based on plasmonic nanostructures: a review, Proc. IEEE 104 (2016) 2380–2408, https://doi.org/10.1109/JPROC.2016.2624340.
[26] S. Hageneder, S. Fossati, N.-G. Ferrer, B. Güngörmez, S.K. Auer, J. Dostalek, Multi-diffractive grating for surface plasmon biosensors with direct back-side excitation, Opt. Express 28 (2020) 39770, https://doi.org/10.1364/OE.410416.
[27] M. Piliarik, J. Homola, Surface plasmon resonance (SPR) sensors: approaching their limits? Opt. Express 17 (2009) 16505, https://doi.org/10.1364/OE.17.016505.
[28] Techniques for Signal Analysis in Surface Plasmon Resonance Sensors, in: R. S. Marks, I. Abdulhalim, R.S. Marks, I. Abdulhalim (Eds.), Nanomaterials for Water Management, Jenny Stanford Publishing, 2015, pp. 175–198, https://doi.org/10.1201/b18715-9, 0 ed.
[29] K. Johansen, R. Stålberg, I. Lundström, B. Liedberg, Surface plasmon resonance: instrumental resolution using photo diode arrays, Meas. Sci. Technol. 11 (2000) 1630–1638, https://doi.org/10.1088/0957-0233/11/11/313.
[30] G.G. Nenninger, M. Piliarik, J. Homola, Data analysis for optical sensors based on spectroscopy of surface plasmons, Meas. Sci. Technol. 13 (2002) 2038–2046, https://doi.org/10.1088/0957-0233/13/12/332.
[31] N. Granqvist, A. Hanning, L. Eng, J. Tuppurainen, T. Viitala, Label-enhanced surface plasmon resonance: a new concept for improved performance in optical biosensor analysis, Sensors 13 (2013) 15348–15363, https://doi.org/10.3390/s131115348.
[32] P. Chen, N.T. Tran, X. Wen, Q. Xiong, B. Liedberg, Inflection point of the localized surface plasmon resonance peak: a general method to improve the sensitivity, ACS Sens 2 (2017) 235–242, https://doi.org/10.1021/acssensors.6b00633.
[33] M. Toma, Y. Itakura, S. Namihara, K. Kajikawa, Sensitive label-free immunoassay by colorimetric plasmonic biosensors using silver nanodome arrays, Adv. Eng. Mater. 25 (2023) 2200912, https://doi.org/10.1002/adem.202200912.
[34] P. Giacomini, O. Segatto, P.G. Natali, Multiple epitope recognition: an approach to improved radioimmunodetection of tumor-associated antigens, Int. J. Cancer 39 (1987) 729–736, https://doi.org/10.1002/ijc.2910390613.
[35] Y.-S. Wang, S. Yau, L.-K. Chau, A. Mohamed, C.-J. Huang, Functional biointerfaces based on mixed zwitterionic self-assembled monolayers for biosensing applications, Langmuir 35 (2019) 1652–1661, https://doi.org/10.1021/acs.langmuir.8b01779.
[36] I. Inou, M. Fujimoto, K. Bando, Anticrossing behavior in nanolayered heterostructures caused by coupling between a planar waveguide mode in an anthracene single crystal and a silver surface plasmon polariton mode: implications for attenuated total reflection spectroscopy, ACS Appl. Nano Mater. 4 (2021) 250–259, https://doi.org/10.1021/acsanm.0c02571.
[37] X. Wang, T. Osada, Y. Wang, L. Yu, K. Sakakura, A. Katayama, J.B. McCarthy, A. Brufsky, M. Chivukula, T. Khoury, D.S. Hsu, W.T. Barry, H.K. Lyerly, T.M. Clay, S. Ferrone, CSPG4 protein as a new target for the antibody-based immunotherapy of triple-negative breast cancer, JNCI: J. Natl. Cancer Inst. 102 (2010) 1496–1512, https://doi.org/10.1093/jnci/djq343.

Roger Hasler obtained his Master degree in Chemistry from the Swiss Federal Institute of Technology (ETH) Zurich in 2016 and continued his research activities as research assistant in the Laboratory for Functional Inorganic Materials at ETH. In 2017 he joined the Center for Radiopharmaceutical Sciences at the Paul Scherrer Institute in Villigen as technical specialist in the Radionuclide Development group. In October 2019, he moved to the Austrian Institute of Technology in Vienna as PhD candidate in the H2020-MSCA-ITN BORGES program. In 2023 he joined the Danube Private University and as researcher in the Laboratory for Life Sciences and Technology (LiST) in Wiener Neustadt.

Dario Cattozzo Mor obtained his Master degree in Nanotechnologies for ICTs from the Polytechnic University of Turin in 2020, carrying out his thesis project in the Quantum Nanostructures and Nanofabrication Group of the Massachusetts Institute of Technology. Since 2021, he has been a PhD student at the Institute of Physics of the Czech Academy of Sciences. His research focuses on plasmonic nanostructures in combination with responsive polymer materials for biosensing and microactuation applications.

Gizem Aktug, who earned her Master's degree in Molecular Biology and Genetics from Gebze Technical University in 2019, is since 2023 a PhD student at Charles University specializing in Biophysics, Chemical, and Macromolecular Physics. Her current research at the Institute of Physics CAS focuses on developing affinity optical biosensors for continuous monitoring and single molecule detection.

Stefan Fossati studied physics at the University of Technology Vienna and joined the Austrian Institute of Technology in 2015 where he since pursued his research activities as PhD and PostDoc in the group of Jakub Dostalek. Since 2019 he is lecturer at the IMC University of Applied Science Krems, Austria and in 2023 he acquired a postdoc position at Institute of Physics, Czech Academy of Sciences in Prague. His research interest focuses on nanophotonics, in particular plasmonics, for biosensor applications.

Van Truc Vu received her M.D. (Medical Doctor) degree of General Medicine in 2017 from the Pham Ngoc Thach University of Medicine in Ho Chi Minh City, Vietnam and M.S. (Master of Science) in 2022 from the National Central University in Taoyuan, Taiwan. She is currently a Ph.D. (Doctor of Philosophy) student since 2022. Her research focuses on the synthesis and characterization of functional silanes/silatranes for diverse applications (surface functionalization, sol-gel synthesis, polymerization).

Adrián Tamayo graduated in Physics and Chemistry at Autonomous University of Barcelona, Spain, in 2016. He received his Ph.D. in Materials Science at NANOMOL in the Institute of Materials Science (ICMAB-CSIC) at the Autonomous University in Barcelona, Spain, in 2022. After the Ph.D., he joined the Institut de Science et d'Ingénierie Supramoléculaires (ISIS), Strasbourg, as a postdoctoral fellow. His current research interests include organic electronics, optoelectronic applications, organic semiconductors, 2D materials, charge transport, and sensors.

Elena Giordani obtained her PhD in Biomedical sciences and biotechnology at the University of Ferrara in October 2021 with a thesis entitled "Liquid Biopsy in Real Life Oncology". Since 2021, she has been senior researcher in the Translational Oncology Research Unit of the IRCSS Regina Elena National Cancer Institute in Rome. Her research focuses on innovative liquid biopsy-based approaches to improve clinical outcome and therapeutic approach in breast cancer and melanoma patients.

Elena Ricciardi obtained her Master degree in Medical Biotechnologies at the University of Tor Vergata, Italy, in 2019. After that she joined the Biogem protein Factory in Ariano Irpino, Italy. Since 2023 she acquired a senior position as a translational researcher in the Translational Oncology Research Unit of the IRCSS Regina Elena National Cancer Institute in Rome. Her work is based on longitudinal monitoring of breast and melanoma cancer patients by liquid biopsy methods.

Patrizio Giacomini obtained his specialty degree in Infectious Diseases and Immunology in 1985. Scripps Clinic & Research Foundation, La Jolla, CA: Visiting AIRC Fellow. 1981. Columbia University, New York USA, Department of Pathology, Junior Assistant Professor, 1982–1984. IRCCS National Cancer Institute Regina Elena (IRE), Immunology Laboratory: AIRC Fellow, 1984–1987. Italian National Cancer Institute, Genova: Assistant Professor, 1987. Vice-Director, Immunology Lab, IRE, 1989–1998. Visiting Fellow, the National Institutes of Health, Bethesda, MD USA, 1996. Head, Immunology Laboratory, IRE, 1998–2016. Staff, Oncogenomics and Epigenetics, Member of the MTB, IRE, 2016–2023. Head, Clinical Trial Center, IRE, 2021–2023.

Jiri Perutka received his doctorate in 1996 from the Masaryk University in Brno. After his postdoctoral training at the Texas A&M University in College Station, he accepted a research associate position at the Institute for Cellular and Molecular Biology and Department of Molecular Biosciences, The University of Texas at Austin, where he developed an algorithm for computer design of group II introns ("targetrons") broadly applied in genetic and metabolic engineering. Since 2019, Jiri has been working as a bioinformatician at Procomcure Biotech GmbH.

Kamil Onder is a CEO of Procomcure Biotech GmbH in Salzburg Thulgau, Austria and has experience in design and development of genetical recombinant peptide libraries and is an expert in numerous protein / peptide interaction systems (Yeast 2-hybrid, one-hybrid, mammalian 2-hybrid, phage-display, ribosome display, fragment complementation, pull-down/co-IP precipitation and more) and biological detection technologies.

Christoph Kleber is a full professor of chemistry at the DPU Krems. He received his diploma in Physical and Theoretical Chemistry in 1999 and his doctorate in Analytical Chemistry at the Vienna University of Technology in 2002. He was appointed Professor of Biotechnology at the University of Applied Sciences Krems in 2005 and habilitated in Materials Science in 2009. In 2010, he was appointed Scientific Director and Managing Director of the Austrian Competence Center for Electrochemical Surface Technology in Wiener Neustadt. He has been a visiting professor at the JKU Linz at Prof. Hassel's institute since 2016 and at the DPU since 2019. His scientific work focuses on the interface between different materials and their ambient atmosphere to elucidate the mechanisms of (bio) degradation at the molecular level in relation to sensor materials.

Paolo Samorì is Distinguished Professor at the University of Strasbourg and Deputy Director of the Institut de Science et d'Ingénierie Supramoléculaires (ISIS). He has obtained a Laurea in Industrial Chemistry at University of Bologna in 1995 and a PhD in Chemistry at the Humboldt University of Berlin in 2000. He was permanent research scientist at Istituto per la Sintesi Organica e la Fotoreattività of the CNR of Bologna. His current research interests comprise 2D materials, supramolecular chemistry, responsive interfaces, and development high-performance multifunctional materials and (nano)devices for energy, sensing and optoelectronic applications.

Chun-Jen Huang is currently the Distinguished Professor of Chemical & Materials Engineering at the National Central University (NCU), Taiwan. He received his B.S. degree in 2001 from Chang Gung University, M.S. in 2003 from the National Taiwan University, and Ph.D. from Johannes Gutenberg Universität Mainz, Germany in 2010 under the guidance of Prof. Wolfgang Knoll and Dr. Jakub Dostalek. He was a postdoctoral fellow at the University of Washington, Seattle with Prof. Shaoyi Jiang in 2011. Prof. Huang's research focuses on biomolecular interfaces, biomaterials, and biosensors–particularly on the development of zwitterionic-based functional materials for biomedical and engineering applications.

Jakub Dostalek received his PhD in 2006 from the Charles University in Prague and worked as a research assistant at the Institute of Photonics and Electronics, Czech Academy of Sciences (CAS) until 2006. After his postdoctoral training at Max Planck Institute for Polymer Research in Mainz, he was appointed there as a project leader and in 2009 he moved to the Austrian Institute of Technology in Vienna, where he served a senior scientist position from 2015 to 2023. Since 2020, he is a lecturer at the University of Natural Resources. In 2021, he assumed senior researcher position at the Institute of Physics CAS in Prague and from 2023 he is group leader at Danube Private University in Wiener Neustadt.